Electrical and optical characterization of a pulsed discharge in immiscible layered liquids: n-heptane and water with various electrical conductivity

Ahmad Hamdan* and James Diamond

Groupe de physique des plasmas, Département de Physique, Université de Montréal,

1375 Avenue Thérèse-Lavoie-Roux, Montréal, H2V 0B3, Québec, Canada

*corresponding author. Email: ahmad.hamdan@umontreal.ca

Keywords: nanosecond discharge, plasma in water, water-heptane interface, streamer-to-spark transition, ICCD imaging.

ABSTRACT

In-liquid pulsed nanosecond discharges produce highly dynamic plasmas that can be applied in different fields. In this study, we investigate the discharge dynamics of plasmas generated at or near the interface of water (with various electrical conductivities) and liquid heptane. The results indicate that at low conductivity (≤ 100 μS/cm), the discharges are most successful when the anode tip is in water and close to the interface. At these conditions, the plasma shape is filamentary, i.e. streamer-like. Meanwhile, at high conductivity (≥ 500 μS/cm), the highest percentage of successful discharges is observed for the case where the anode tip is in heptane, near the interface. The plasma generated at these conditions takes the shape of one wide and intense filament, i.e. spark-like. The transition from streamer-to-spark mode is also confirmed by electrical and optical measurements. Using a negative polarity, the highest percentage of successful discharges generated in low-conductivity water in water near the interface. When the conductivity is increased, the success rate of discharges attains 100%, if the cathode pin is kept in water.

1. INTRODUCTION

Despite their great potential in various fields [1–4], the application of discharges in liquid is limited by the ambiguity of the complex plasma dynamics. In-liquid discharges are commonly produced by applying a pulsed high voltage with relatively short rising slope (~1 kV/ns) [5,6]. Longer slopes lead to the formation of bubbles in which the discharge ignites [7,8]. The plasma filaments and streamers produced by in-liquid discharges propagate from the the tip of the high-voltage electrode into the liquid [9,10]. Based on previous studies, discharges in liquid are highly sensitive to experimental conditions, especially the liquid nature (polar or non-polar), electrode geometry, hydrostatic pressure, and volatge characteristics (magnitude, polarity, and pulse duration) [11–13]. The properties of in-liquid streamers (radius, length, lifetime, degree of filamentation, etc.) are also dependent on the experimental conditions. For example, the streamers generated under positive polarity conditions are filamentary-like, and they are thinner, longer, and faster than the bushy-like streamers produced under negative polarity [10,14]. Such fundamental differences are mainly due to the nature of the charged species in the streamer head and to the formation of space charge, i.e. space electric field [15]. These properties, among others, have raised the interest of the scientific community in in-liquid discharges to great extent.

The unique properties of in-liquid plasmas, including high pressure and high density of reactive species [16–18], render them useful in numerous technological applications [19–21]. For example, the oxidative species (O*, OH, O_3, H_2O_2, etc.), energetic photons (UV and VUV), shock waves, and cavitation produced by discharges in water [22–24] can induce water sterillization and viruses deactivation/destruction. However, the efficiency of this activity is limited by the relatively reduced plasma volume. To overcome this limitation, researchers have proposed to increase the volume (or the surface of interaction) by sustaining a discharge in gas phase in-contact with water.

This way, the reactive species are abundantly produced in the gas phase and at the liquid surface, then they diffuse in the liquid [25–27]. Alternatively, the plasma efficiency may be enhanced by injecting gaseous bubbles in the liquid and initiating the plasma in these bubbles using a high-volatge discharge [28–31] or microwave power [32–34]. According to previous studies, the bubbled liquid system implicates an important phenomenon — electric field intensification — that occurs at the gas/liquid interface due to the discontinuity of dielectric permittivity [35–38]. Electric field intensification may also occur at the inteface of two immiscible liquids that have different dielectric permittivities. So far, this phenomenon has been investigated in two systems of immiscible layered liquids: water-heptane [39,40] and water-organosilicon liquid (hexamethyldisiloxane) [41]. The reported results demonstrate that greater differences between the dielectric permittivities of the two liquids induce higher intensification of the electric field, which facilitates the occurrence of the discharges.

Motivated by our recent investigations on the subject of immiscible layered liquids (water-heptane) [39–41], we study herein the influence of water conductivity (10-5000 μS/cm) and voltage polarity on discharge probability and properties. The effect of distance between the electrode tip and the water/heptane interface on the probability of the discharge is also assessed. The electrical characteristics, emission morphology, and optical emission properties of the discharge are analyzed under the various experimental conditions.

2. EXPERIMENTAL SETUP

As shown in Figure 1, a nanosecond positive/negative pulsed power supply (NSP 120-20-P/N-500-TG-H, Eagle Harbor Technologies) was used to generate electrical discharges in liquid solutions. The pulse width and voltage magnitude were fixed at 500 ns and 22 kV, respectively.

To avoid discharge-discharge interactions, all experiments were conducted at the relatively low repetition rate of 5 Hz. A tungsten rod (diameter of 2 mm, Goodfellow) with a mechanically polished tip (curvature radius of ~10 µm) was mounted on a micrometer positioning system and used as anode. Another tungsten rod (diameter of 4 mm, Goodfellow) was placed at the bottom of a cylindrical quartz cell (diameter of 2 cm, thickness of 1 mm) filled with solutions and used as cathode. To avoid spark discharge between the two metal electrodes, he gap distance between them was kept above 2 cm.

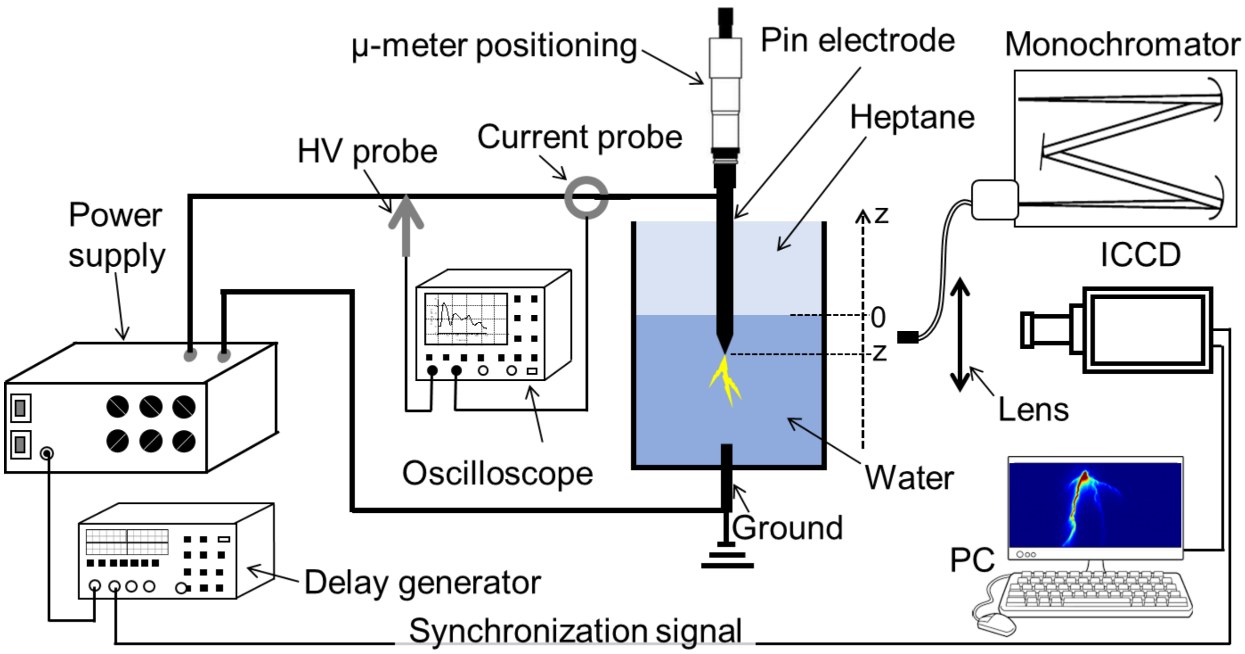

Figure 1. *Scheme of the experimental setup used to produce pulsed nanosecond discharges in solutions.*

The quartz cell is filled with 20 mL of the electrolyte (distilled water + KCl) and 10 mL of n-hepatne (note that the relative volume of both liquids does not affect the reported results). Considering that the density of water (1 g/cm^3) is greater than that of n-heptane (0.68 g/cm^3), the latter lied of top of the former. The electrical conductivity of water was adjusted by adding KCl, and the tested conductivity values were 10, 50, 100, 500, and 5000 µS/cm. The experiments were performed under positive and negative voltage polarities, at conditions where the anode tip is at the heptane/water interface (z = 0), in water (z < 0), or in heptane (z > 0).

The electrical characteristics (voltage and current) of the discharges examined in this study were measured using a high-voltage probe (P6015A, Tektronix) and a current monitor (6585, Pearson), respectively. Voltage and current waveforms were visualized and recorded using an oscilloscope (MSO54, 2 GHz, 6.25 GS/s). An ICCD camera (PIMAX-4: 1024 EMB, Princeton Instruments) was used to monitor plasma emission behavior. The camera is equipped with an intensifier type RB that covers the wavelength range of 200-850 nm has a quantum efficiency between 2 and 15%, depending on the wavelength. The integration time was set to 1.5 µs. A delay generator (Quantum Composers Plus 9518 Pulse Generator) was used to ensure synchronization between the ICCD camera and the voltage pulse. A monochromator (Acton 2750) was employed to analyze plasma radiation. The intensity of each optical transition was recorded by an ICCD camera (PIMAX from Princeton Instruments). Light emission measurements were carried out using the 300 lines/mm grating blazed in the visible range.

3. RESULTS

3.1. Positive Polarity

3.1.1. Effect of gap distance on discharges in heptane/distilled water

The percentage of successful discharges was determined based on the detection of light emission using an ICCD camera. For this purpose, the discharges at each experimental condition were generated by applying 500 pulses at the repetition rate of 5 Hz, and the ICCD camera recorded the light emission around the pin electrode (integration time of 1.5 µs) for each pulse. The acquired images were processed, and the percentage of successful discharges was determined. Figure 2a shows variations in the percentage of successful discharges in distilled water (~10 μS/cm) as a function of interface-pin distance (z). When the pin is in water, far from the interface (z < - 4 mm), no discharge occurs. At -4 mm < z < -1 mm, the percentage of successful discharges is small; however, it increases as the pin approaches the interface (-1 mm < z < 0), until it reaches ~80% at the interface (z = 0). Once the pin crosses the interface to the heptane side, the discharges cease to occur. As shown in Figure 2b, the voltage waveforms recorded at z = -4 mm (pin in water, no discharge), z = 0 mm (pin at the interface, highest percentage of successful discharges), and z = 2.5 mm (pin in heptane, no discharge) are similar, and none of them exhibits a drop (i.e. no breakdown). Meanwhile, the current waveforms measured at these conditions (Figure 2c) present a principal peak at t ~0 corresponding to the displacement current (because no discharges were occurred at z = -4 and 2.5 mm) induced by the rise of voltage. As expected, the value of this peak changes with gap distance due to the variation of the gap capacitance. At z = 0 mm, when many discharges occur, a series of current peaks with values between 0.1 and 0.2 A is detected within the time period of 200-500 ns.

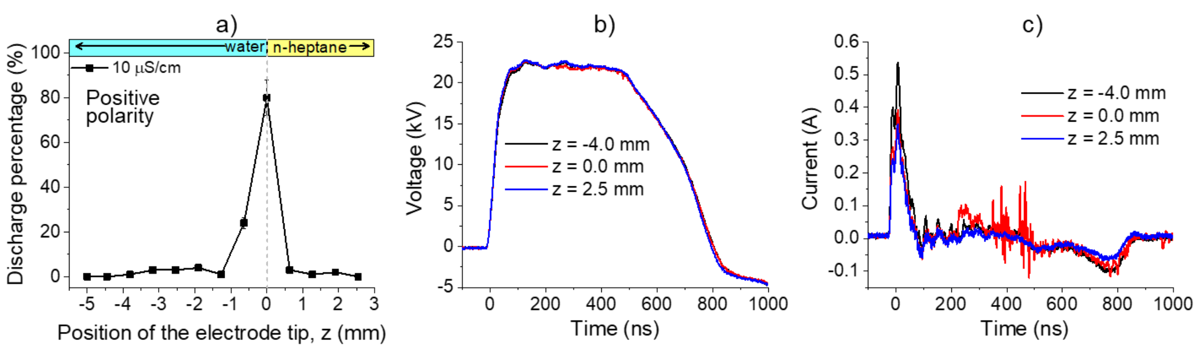

Figure 2. *a) Variation of the percentage of successful discharges (positive polarity) in distilled water (conductivity of 10 μS/cm) as a function of z. b) Voltage and c) current waveforms of typical discharges at in distilled water (conductivity of 10 μS/cm) at different gap distances.*

The ICCD images shown in Figure 3 demonstrate that, in water, discharges start to occur at z = -2.5 mm, with no discharges detected further away from the interface. The discharge emission at this gap distance is filamentary in shape and has a relatively short length (~0.5 mm). As the anode tip approaches the interface (z = -1.9, -1.3, and -0.6 mm), the number, intensity, and length of plasma filaments increases. At z = 0 mm, the filaments are even lengthier; however, instead of propagating towards the cathode (the bottom of the cell), they propagate horizontally, which means that they are influenced by the interface.

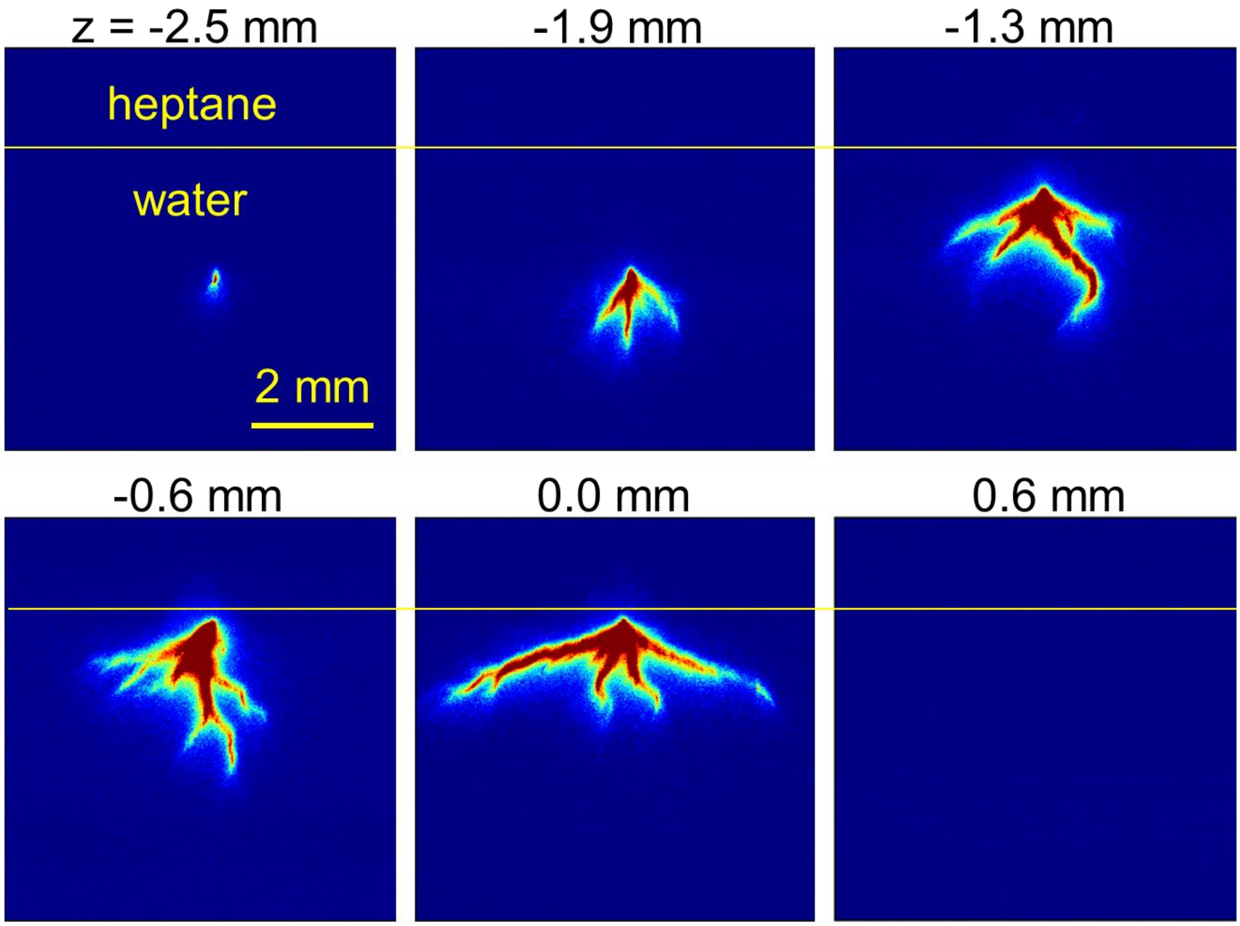

Figure 3. *ICCD images (1.5 µs integration) showing the discharge emissions (positive polarity) produced in distilled water (conductivity of 10 µS/cm) at various z. The heptane/water interface is indicated by a yellow line.*

3.1.2. Effect of electrical conductivity and gap distance on discharges in heptane/water

When the conductivity of water is increased beyond 10 µS/cm, more discharges occur in water, far from the interface (Figure 4a). At 50 and 100 µS/cm, ~80% successful discharges is observed at z = -2 and -1.2 mm, respectively, and 100% success is achieved at the interface (z = 0 mm). Above the interface (z = 0.6 mm), in heptane, ~40% of discharges are successful. Further increasing the conductivity of water to 500 µS/cm leads to even higher probabilities of successful discharges, but only at distances very near to the interface, in the water side (z = -0.6 and 0 mm). Such a non-monotonous behavior can be explained by the combination of two phenomena. The first phenomenon is related to the decrease of discharge probability as water conductivity is increased, because of the presence of free ions in water. The second phenomenon is related to the intensification of the electric field at the electrode tip. Indeed, for a given voltage, as the electrode tip approaches the interface, the electric field at the tip is significantly enhanced (see Figure 9 and the Discussion section), which compensates the decrease of discharge occurrence due to a conductivity increase. The convolution of these two phenomena explain the non-monotonous behavior of the discharge occurrence.

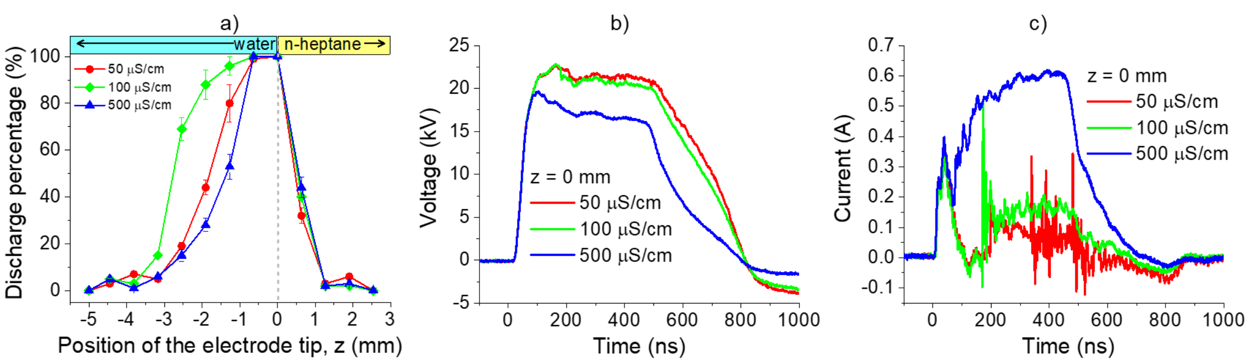

Figure 4. *a) Variation of the percentage of successful discharges (positive polarity) in water as a function of z, at various electrical conductivities (50, 100, and 500 µS/cm). b) Voltage and b) current waveforms of typical discharges at the heptane/water interface (z = 0) under various conductivity conditions.*

As shown in Figure 4b, the voltage waveforms of discharges generated at the interface (z = 0 mm) under conductivity conditions of 50 and 100 µS/cm are relatively similar, and they both present a drop of ~2 kV at t ~200 ns. At 500 µS/cm, the profile is significantly different, and the voltage plateaus at ~20 kV instead of ~22 kV. Moreover, the voltage drop at this condition increases to ~4 kV. As for the current waveforms (Figure 4c) recorded at 50, 100, and 500 μS/cm, they show similar displacement current peaks, but different discharge current peaks. The discharge current at 500 μS/cm is higher than that detected at 100 μS/cm, which in turn is greater than the current at 50 μS/cm. Notably, many spikes are observed at the lower electrical conductivities, but not at 500 μS/cm. This behavior is related to a change in the discharge mode, as discussed below.

ICCD images of the plasma emissions produced under varying conditions of z and electrical conductivity were recorded and are shown in Figure 5. Based on these images, the emissions generated far from the interface at 50 and 100 μS/cm are characterized by few plasma filaments with lengths of ~1 mm. As the electrode tip approaches the interface, the plasma filaments become longer and more intense, and at the interface (z = 0 mm), horizontally-propagating filaments (i.e. influenced by the interface) are observed, in addition to those propagating towards the cathode. Notably, the vertical filaments are longer than the horizontal ones, unlike the case of 10 μS/cm conductivity. A little above the interface (z = 0.6 mm), the probability of successful discharge is low (Figure 4a), and the emission patterns (filaments) of the discharges that occur are similar to those observed in water. However, the lengths of the vertical filaments detected in heptane are significantly less than those of the horizontal ones.

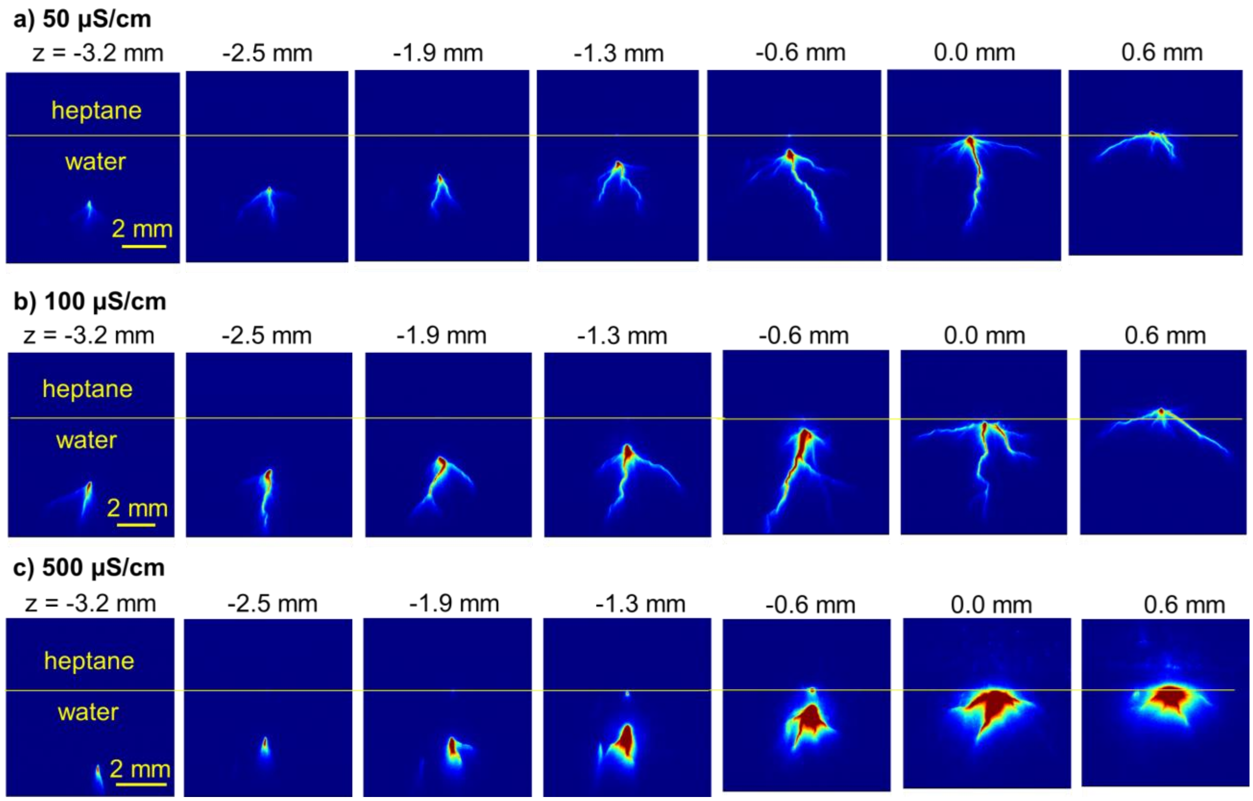

Figure 5. *ICCD images (1.5 µs integration) showing the discharge emissions (positive polarity) produced in water at a) 50, b) 100, and c) 500 µS/cm, and various gap distances. The heptane/water interface is indicated by a yellow line.*

At 500 µS/cm, the filamentation phenomenon is significantly suppressed (Figure 5c). Compared to the lower conductivity cases, the filaments observed at 500 µS/cm are more intense, shorter, and wider. Consequently, the emission is more localized in the solution, close to the electrode's tip. At z = 0.6 mm, the filaments are short, and the emission zone seems to be elliptical-like instead of filamentary-like.

Further increasing the conductivity to 5000 µS/cm leads to fewer successful discharges in water, far from the interface, with ~90% probability of success at the interface (Figure 6a). Interestingly, the probability increases to 100% in heptane (z = 0.6 mm). As for the voltage and current characteristics of the discharges achieved at 5000 µS/cm, they are similar to those observed at 500 µS/cm, as shown in Figure 6b. The ICCD images presented in Figure 6c show that at 5000 μS/cm, filamentation is totally suppressed, and only one plasma emission zone is observed. At z = -0.6 mm, the emission intensity is relatively low; however, it increases significantly and takes an elliptical-like shape when the anode tip is at the interface (z = 0). In heptane (z = 0.6 and 1.3 mm), the discharge emission is much more intense, and it is concentrated in one single wide channel (~1 mm).

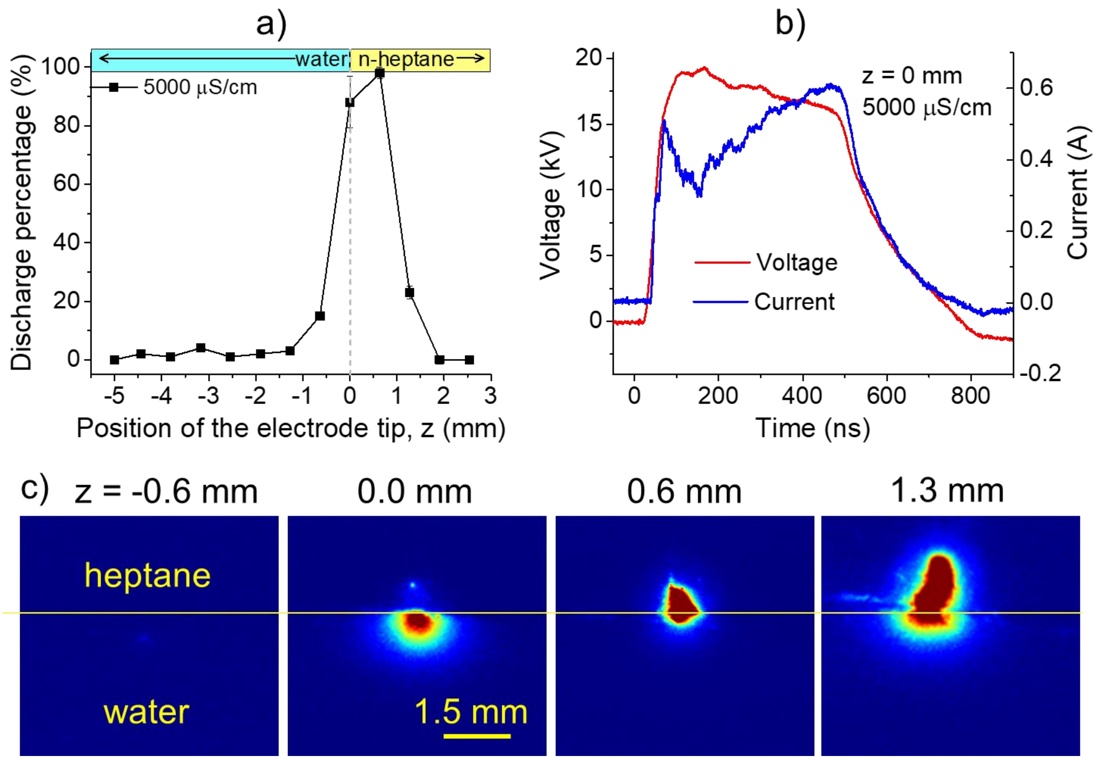

Figure 6. *a) Variation of the percentage of successful discharges (positive polarity) produced in water as a function z, at 5000 μS/cm. b) Voltage and current waveforms of a typical discharge generated at the heptane/water interface (z = 0), at 5000 μS/cm. c) ICCD images (1.5 μs integration) showing the discharge emission in water at 5000 μS/cm and various z. The heptane/water interface is indicated by a yellow line.*

3.2. Negative Polarity

The discharge probability and emission morphology were also investigated under negative polarity voltage conditions. Like in the case of positive polarity, the effect of z on the percentage of successful discharges was analyzed. As shown in Figure 7a, the probability of success increases as the cathode pin approaches the interface, when water conductivity is 10-500 µS/cm. Moreover, the spatial range (z) of the discharge broadens with increasing conductivity. Although these results are similar to those observed under positive polarity, a clear dependence on voltage polarity is detected at 5000 µS/cm. In negative polarity mode, the probability of discharge is 100% as long as the cathode pin is in water (i.e. $z < 0$). However, in heptane ($z > 0$), the probability is 0%. Meanwhile, the percentage of successful discharges is significantly decreased in water under positive polarity conditions, and it reaches 100% in heptane at $z = 0.6$ mm (Figure 6a).

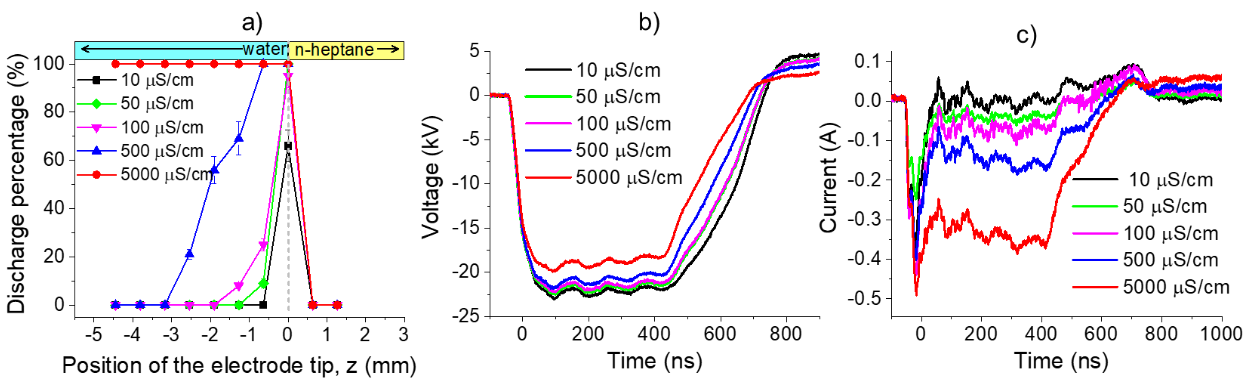

Figure 7. *a) Variation of the percentage of successful discharges (negative polarity) produced in water as a function z, under various electrical conductivities (10, 50, 100, 500, and 5000 µS/cm). b) Voltage and c) current waveforms of typical discharges generated at the heptane/water interface (z = 0) under various electrical conductivities.*

The electrical characteristics (Figures 7b and 7c) detected at negative polarity are fairly different from those acquired in positive polarity. When the voltage is negative, some oscillations in the waveforms are observed, but no current spikes are detected (they are detected at positive polarity). Although the current increases with increasing electrical conductivity, the values measured at negative polarity are relatively smaller than those determined at positive polarity, especially at higher conductivity conditions. For instance, at 5000 µS/cm, the peak current is ~0.4 A in negative mode, compared to 0.6 A in positive mode.

The ICCD images shown in Figure 8 demonstrate that at 10 µS/cm, the discharge occurs only at the interface (z = 0) and takes the shape of a single filament (~0.5 mm long) that is relatively wider than the filaments produced under positive polarity. At 50 and 100 µS/cm, the discharge is localized at the cathode tip in water and at the water/heptane interface, with the interface emission being slightly wider and less intense. At 500 µS/cm, an even wider plasma filament is detected. Finally, at 5000 µS/cm, the discharge emits low-intensity light at a distance far from the interface, but it is strongly localized at the cathode tip. As the cathode tip approaches the interface, the discharge emission becomes wider, but surprisingly its length does not significantly change.

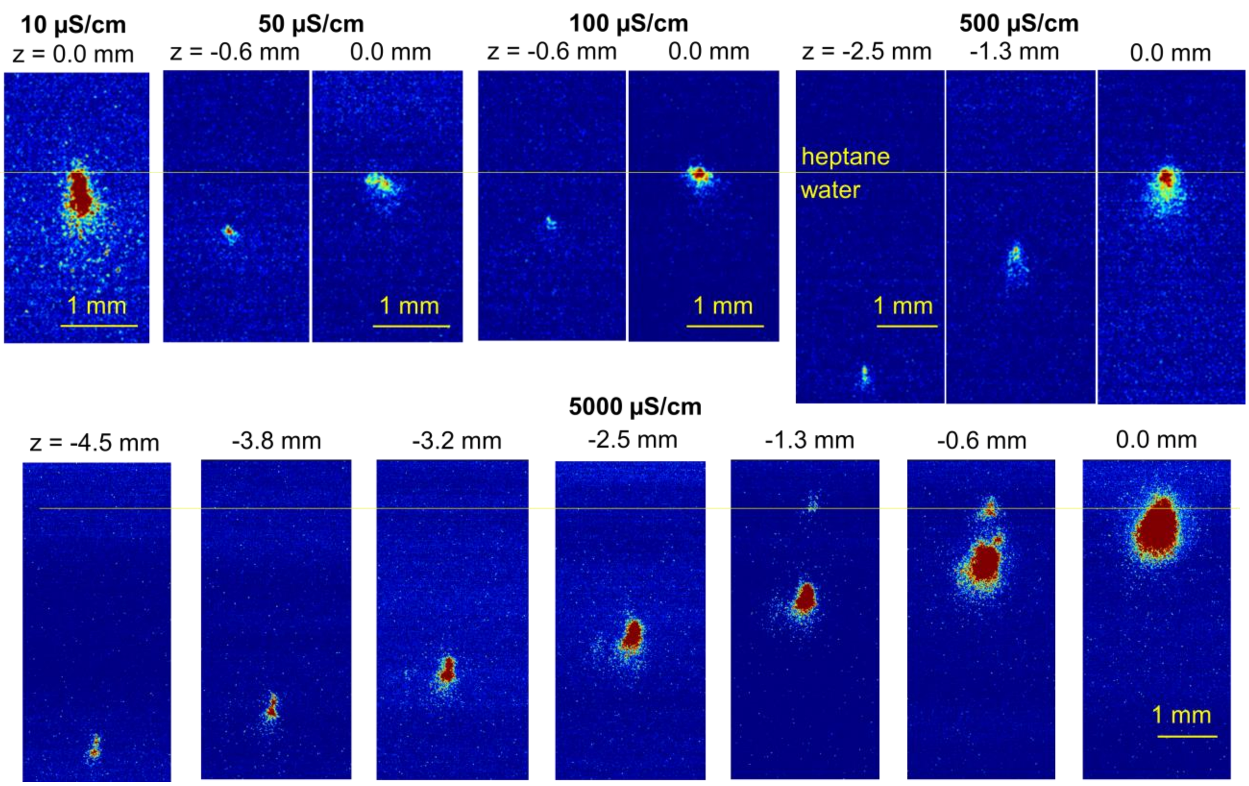

Figure 8. *ICCD images (1.5 µs integration) showing the discharge emission (negative polarity) produced in water under various electrical conductivities (10, 50, 100, 500, and 5000 µS/cm) and at various z. The heptane/water interface is indicated by a yellow line.*

4. DISCUSSION

The results reported in this study indicate that the discharge is sensitive to the gap distance between the electrode tip and the water/heptane interface (z), as well as to the electrical conductivity of water. For a given water conductivity, the percentage of successful discharges increases with decreasing z until it reaches ~100% close to the interface (z = 0). Moreover, the plasma filaments tend to propagate horizontally near to the interface. These observations are attributed to the dependence of the electric field distribution on z. To verify this hypothesis, the electric field distribution was simulated in 2D using the Comsol Multiphisics Software. The experimental radius and curvature of the electrode tip were adopted in the simulation, and the applied voltage was set to 22 kV. The dielectric permittivities (ε) of water and heptane in the lower and upper zones of the simulated regions were taken to be 80 and 2, respectively. Considering that changes in ε_{water} as a function of conductivity are negligible within the range investigated herein [42–44], the permittivity value of 80 is representative of all the different conductivity water solutions analyzed in this study. Also, the simulation was conducted in stationary mode, and thus, the results do not significantly depend on conductivity. Figures 9a and 9b depict the simulated electric field distribution and evolution of the electric field value at the electrode tip as a function of z, respectively. Based on these figures, when the pin is in water ($z < -1$ mm), the field value is ~6-7 × 10^7 V/m, which is similar to the value determined for a discharge in water only (not shown here). This indicates that when the electrode is far from the interface, the effect of heptane on the electric field at its tip is not significant. As the tip approaches the interface ($-1 < z < 0$ mm), the electric field increases rapidly to reach a maximum of ~10^9 V/m at z = 0 mm, which explains the increase of discharge probability as the electrode tip approaches the interface. In addition, the field distribution zone broadens near the interface where the electric field is high (-1 mm $< z < 0$ mm), which explains the horizontal propagation of filaments. In fact, streamer propagation in multiphase media has been intensively studied in the context of discharges in bubbles in liquids [29-31, 35-37]. For instance, Babaeva and Kushner [35] have investigated streamer propagation in bubbles in liquids under different conditions. Despite the difference between the two situations of gas-liquid interface and liquid-liquid interface, a lot of similarities exist. Indeed, the electric field distribution is heavily influenced by ε of the medium. Considering that ε of a gas (~1) is comparable to that of heptane (~2), the results reported in [35] can be extrapolated to our study, at least from a qualitative perspective. Previously, it has been demonstrated that in the case of two media with different ε (80 for water and 1 for gas), the streamer tends to propagate along the gas-liquid interface. Therefore, it is expected that in the case of water-heptane, streamer propagation will also be along the interface, i.e. horizonal, as the images have showed. This can be mainly explained by the refraction of the electric field lines on the interface which reduces the vertical electric field. Moreover, as mentioned in [35], as soon as the streamer is initiated close to the interface, a gradual screening of the electric field in water helps to supress the development of vertical streamers and supports horizontal propagation.

In heptane ($z > 0$), the electric field decreases. Notably, the values are not symmetrically distributed with respect to the interface. For instance, at $z = +0.5$ and -0.5 mm, the electric field is 4.5×10^8 and 8×10^7 V/m, respectively. Such non symmetric behavior is expected as the dielectric permittivities of the two media are different.

The increase of the probability of successful discharges (positive polarity) near the interface, in heptane, is attributed to the relatively high electric field. At high conductivity, the K^+ and Cl^- ions may be considered as an extended ground, which promotes discharges in heptane ($z > 0$) between the anode tip and the interface. These discharges are similar to those formed between two metal electrodes — spark discharges — immersed in heptane.

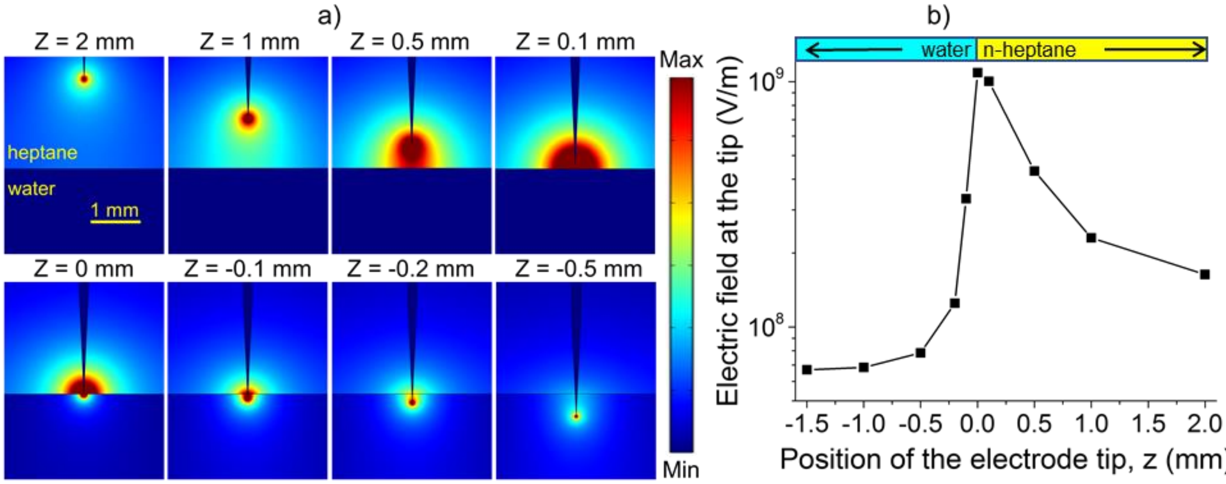

Figure 9. *a) Numerical simulations of the electric field intensity distribution at different z. Distilled water is at the bottom, and heptane is on top. b) Variation of maximum electric field at the electrode tip as a function of z.*

Based on the experimental results, the discharge properties (voltage, current, and emission morphology) at the interface are significantly influenced by the conductivity of water. To quantitatively assess the variations in the electrical characteristics of the discharge, the current was integrated over time (after applying the displacement current correction), and the injected charge was calculated. The obtained results demonstrate that for positively polarized discharges, the charge is ~0.2 µC at conductivity < 100 µS/cm and ~2.2 µC at a conductivity > 500 µS/cm (Figure 10). Interestingly, the recorded ICCD images (insets in Figure 10) also highlight the significant variations between low- and high-conductivity conditions. Based on the injected charge values and the discharge emission profiles, it is suggested that the discharge propagates in streamer and spark modes at low (≤ 100 µS/cm) and high conductivity (≥ 500 µS/cm), respectively. The in-water streamer discharge reported in this study is very similar to the in-liquid streamers discussed in the literature [6,45–47]. However, to the best of our knowledge, in-liquid spark discharges have only reported been successfully generated between two submerged electrodes, an anode and a cathode

[48–50]. Herein, the spark discharge is induced by the high conductivity of the solution, and it is not physically connected to the cathode electrode.

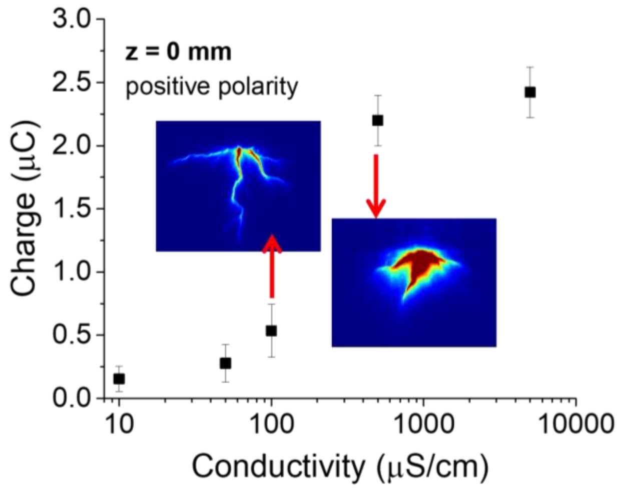

Figure 10. *Variation of the injected charge of discharges (positive polarity) at the water/heptane interface (z = 0) as a function of water conductivity. ICCD images (1.5 μs integration) recorded in low- and high-conductivity zones are shown as insets.*

To further analyze the transition from steamer to spark mode, the optical emission spectra recorded under various conditions of conductivity were integrated over pulse duration and space. As shown in Figure 11a, the spectra are dominated by the emission of three species: C_2 (Swan band from ~480 to 590 nm), H (656.3 nm), and O (777 nm). Interestingly, the Swan band is easily identifiable at low conductivity (≤ 100 μS/cm, i.e. streamer mode), and the vibrational transitions ($\Delta\nu = 1$: ~468-475 nm, $\Delta\nu = 0$: ~506-517 nm, $\Delta\nu = -1$: ~545-565 nm) are clearly visible. However, at higher conductivity (≥ 500 μS/cm, i.e. spark mode), the lines broaden so much that only one broad band is visible.

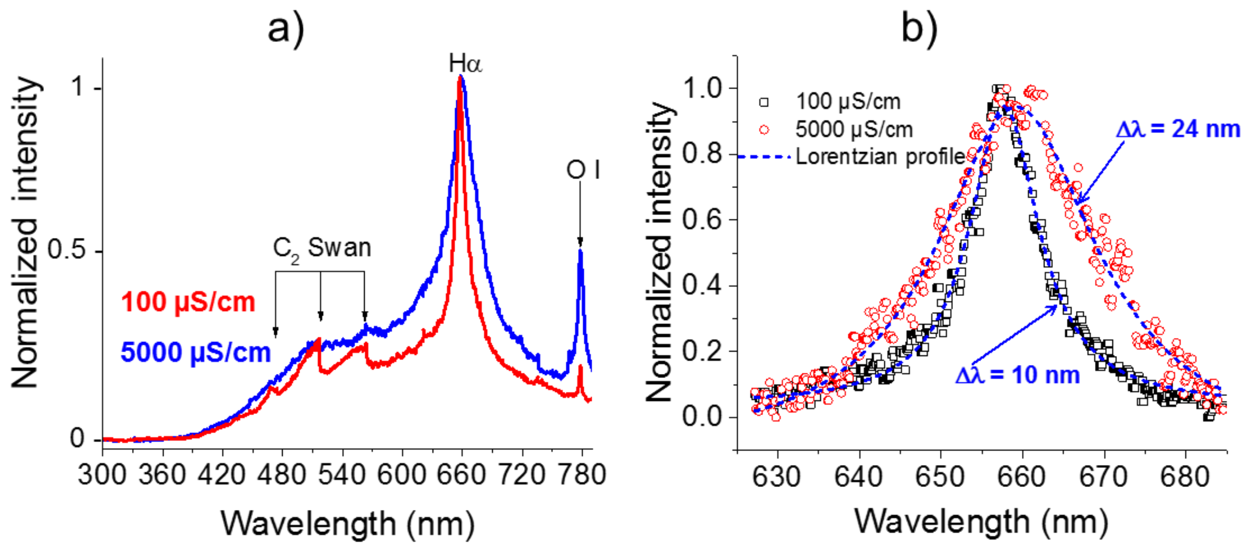

Figure 11. *a) Optical emission spectra (1.5 μs integration) of discharges (positive polarity) at the water/heptane interface (z = 0) for two conductivities: 100 and 5000 μS/cm. b) Hα line profiles and the corresponding Lorentzian fits at 100 and 5000 μS/cm.*

The Hα profiles shown in Figure 11b were used to estimate the electron density in each discharge mode. Despite the elevated temperature and pressure conditions of the spark discharge (several thousands of Kelvins and several tens of bars), the Hα line broadening observed in this discharge mode is mostly attributed to the Stark effect [29,51,52]. Based on this assumption, the experimentally acquired profiles were fitted by Lorentzian functions (Figure 11b). Then, we used the empirical equation linking the electron density (n_e) to full width at half maximum of Hα ($\Delta\lambda$) [53] to determine the former:

$$n_e(cm^{-3}) = 8.83 \times 10^{16} \times \Delta\lambda(nm)^{1.6005} \quad (1)$$

According to equation (1), the electron density in streamer and spark modes is estimated to be 3.5×10^{18} and 1.4×10^{19} cm^{-3}, respectively. These values are in good agreement with those reported in preceding studies for the two modes [46, 48, 54-56], and they vary by almost one order of magnitude, similar to the values of the injected charge. Overall, the results are consistent with the findings of Sunka [57], who uses a different setup (different pulse width and voltage magnitude) to show that an increase in the electrical conductivity of water from 55 to ~500 μS/cm induces a jump of one order of magnitude in electron density (10^{18} to 10^{19} cm^{-3}).

On the other hand, the ICCD images acquired under negative polarity are significantly different from those recorded under positive polarity. In fact, when the voltage is negative, only localized emission is observed, with no filamentation. Moreover, in negative polarity mode, the probability of discharge in highly conductive water, far from the interface, is high, compared to absolutely no discharge in heptane, even at distances close to the interface. Like in the case of positive discharge, the evolution of injected charge as a function of water conductivity was analyzed for negative polarity discharges. As shown in Figure 12a, the initial and final values of the injected charge at 10 and 5000 μS/cm are similar to those determined under positive discharge conditions; however, the evolution profiles are different. Indeed, the charge increase for a positive discharge is stepwise in the conductivity range of 100-500 μS/cm, compared to a smooth and regular increase in the case of negative polarity discharge. Based on the profiles and widths of the Hα lines (656.3 nm) shown in the optical emission spectra of Figure 12b, higher water conductivities induce relatively greater electron densities, which is consistent with the variation of injected charge. However, a detailed comparison of the intensity of the main lines (Hα at 656.3 nm, C_2 Swan ($\Delta\nu = 0$) at ~510 nm, and O at 777 nm) shows that discharges achieved in positive and negative polarity modes are appreciably different.

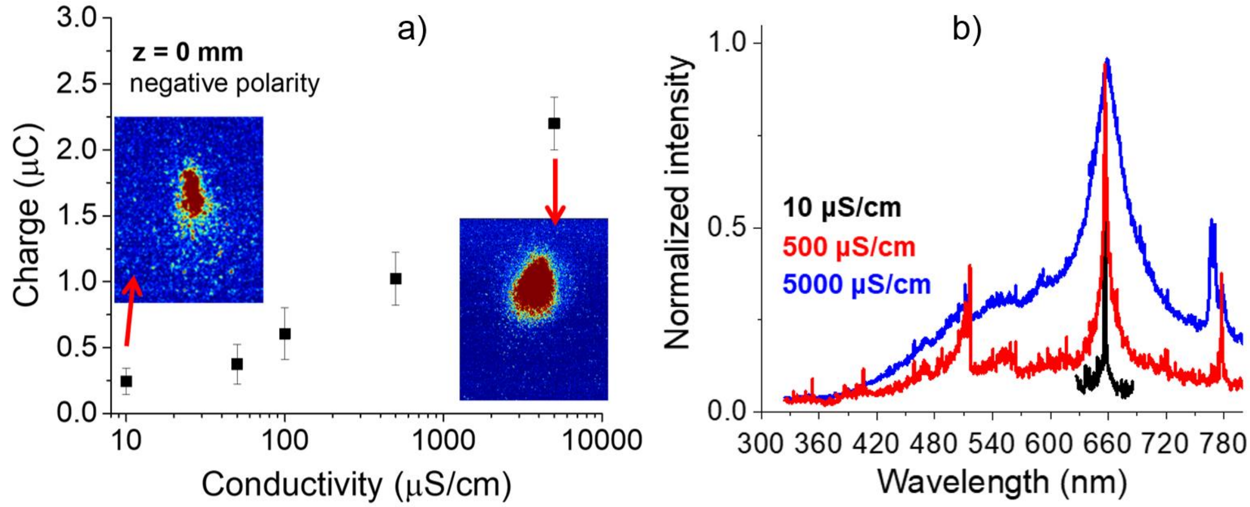

Figure 12. *a) Variation of the injected charge of discharges (negative polarity) at the water/heptane interface (z = 0) as a function of water conductivity. ICCD images (1.5 µs integration) recorded in low- and high-conductivity zones are shown as insets. b) Optical emission spectra (1.5 µs integration) of discharges (negative polarity) at the water/heptane interface (z = 0) for three conductivities: 10, 500, and 5000 µS/cm.*

The behavior of the discharge depends on the nature and flow of carrier charges. Normally, negative discharges exhibit larger breakdown voltages than the positive counterparts [10]. Considering that the voltage amplitude was kept unchanged (~22 kV) for both polarities in this study, it may be assumed that the negative discharges are less 'energetic' than the positive ones. Similarly, previous studies demonstrate that the streamers formed in positive mode are filamentary, whereas those formed in negative mode have thicker root and are bushy in shape [10]. This agrees well with our ICCD images, which show that at low conductivity, the negative streamers are wider than the positive ones. To explain this difference, one must consider that under positive polarity conditions, electrons flow from the liquid towards the anode pin leaving behind a localized positive space charge. At low conductivity, the space charge significantly affects streamer propagation due to the low concentration of free ions in the medium. However, at high conductivity, the space charge influence is reduced by the presence of numerous ions, which explains the absence of filaments and the production of a localized plasma. Meanwhile, in negative polarity, the electrons flow from the cathode pin (probably ejected by field emission) towards the liquid. Therefore, a localized plasma region is expected around the cathode. Beyond this region, the electrons are quickly diluted in the medium due to their high mobility and diffusion, unlike ions. This explains the absence of filamentation and the relatively reduced plasma length. The insignificant dependence of the negative discharge morphology on water conductivity is an interesting feature that has also been reported by Liu et al. [58], albeit at different discharge conditions. Further investigation of the temporal evolution of optical emission is needed to unveil the influence of the heptane layer (or other low-ε liquids) on discharge morphology at different polarities and water conductivities.

To further understand the role of the interface, it is important to identify the ignition mechanisms and plasma propagation dynamics taking place under the investigated conditions. The mechanisms occurring in regions far from the interface, i.e. in water solution ($z < 0$) or in heptane ($z > 0$), are expected to be similar to those previously reported in water only or in liquid hydrocarbon only [5,6, 59]. However, at the interface, the involved mechanisms may be different. As discussed above, the time-integrated optical emission spectra of the discharge ignited at the interface show simultaneous emission of oxygen and carbon species (i.e. dissociation of water and of heptane, respectively). Moreover, the plasma tends to propagate horizontally at the interface, which indicates that the dynamics of propagation in this region is unusual. Further research and characterization using time-resolved techniques (e.g. imaging and optical emission spectroscopy) are needed to investigate this unique plasma dynamic and underlying mechanisms at the interface.

4. CONCLUSION

This study investigates the dynamics and electrical characteristics of a pulsed nanosecond discharge generated in a mixture of water and heptane (low dielectric permittivty liquid). The effects of voltage polarity and water conductivity on the discharge properties are also analyzed. The obtained results demonstrate that when the anode tip (positive polarity) is in water (conductivity ≤ 100 μS/cm), the probability of successful discharge is ~100%. Based on changes in the plasma shape, electrical characteristics, and electron density, it is concluded that the discharge undergoes a transition from streamer mode to spark mode when conductivity is increased in the interval of 100-500 μS/cm. In negative polarity and at low conductivity, the highest percentage of successful discharges is observed in water, close to the interface. However, at high conductivity, the percentage is 100% whenever the cathode pin is in water. Compared to the positive polarity mode, negative polarity plasma emissions are less filamentary, but they exhibit similar values of injected charge and electron density, both of which increase with increasing water conductivity.

ACKNOWLEDGEMENT

The research reported in this publication was financially supported by the Natural Sciences and Engineering Research Council of Canada (NSERC) under award number RGPIN-2018-04869. The authors thank the Fonds de Recherche du Québec – Nature et Technologie (FRQ-NT) and the Canada Foundation for Innovation (CFI) for funding the research infrastructure. A Hamdan acknowledge the Fondation Courtois for the financial support.

REFERENCES

[1] Vanraes P and Bogaerts A 2018 Plasma physics of liquids - A focused review *Appl. Phys. Rev.*

[2] Bruggeman P J, Kushner M J, Locke B R, Gardeniers J G E, Graham W G, Graves D B, Hofman-Caris R C H M, Maric D, Reid J P, Ceriani E, Fernandez Rivas D, Foster J E, Garrick S C, Gorbanev Y, Hamaguchi S, Iza F, Jablonowski H, Klimova E, Kolb J, Krcma F, Lukes P, MacHala Z, Marinov I, Mariotti D, Mededovic Thagard S, Minakata D, Neyts E C, Pawlat J, Petrovic Z L, Pflieger R, Reuter S, Schram D C, Schröter S, Shiraiwa M, Tarabová B, Tsai P A, Verlet J R R, Von Woedtke T, Wilson K R, Yasui K and Zvereva G 2016 Plasma-liquid interactions: A review and roadmap *Plasma Sources Sci. Technol.* **25** 053002

[3] Horikoshi S and Serpone N 2017 In-liquid plasma: a novel tool in the fabrication of nanomaterials and in the treatment of wastewaters *RSC Adv.* **7** 47196–218

[4] Belmonte T, Hamdan A, Kosior F, Noël C and Henrion G 2014 Interaction of discharges with electrode surfaces in dielectric liquids: application to nanoparticle synthesis *J. Phys. D. Appl. Phys.* **47** 224016

[5] Dobrynin D, Seepersad Y, Pekker M, Shneider M, Friedman G and Fridman A 2013 Non-equilibrium nanosecond-pulsed plasma generation in the liquid phase (water, PDMS) without bubbles: fast imaging, spectroscopy and leader-type model *J. Phys. D. Appl. Phys.* **46** 105201

[6] Starikovskiy A 2013 Pulsed nanosecond discharge development in liquids with various dielectric permittivity constants *Plasma Sources Sci. Technol.* **22** 12001

[7] Rond C, Desse J M, Fagnon N, Aubert X, Er M, Vega A and Duten X 2018 Time-resolved

diagnostics of a pin-to-pin pulsed discharge in water: pre-breakdown and breakdown analysis *J. Phys. D. Appl. Phys.* **51** 335201

[8] Rond C, Fagnon N, Vega A and Duten X 2020 Statistical analysis of a micro-pulsed electrical discharge in water *J. Phys. D. Appl. Phys.* **53** 335204

[9] Starikovskiy A, Yang Y, Cho Y I and Fridman A 2011 Non-equilibrium plasma in liquid water: Dynamics of generation and quenching *Plasma Sources Sci. Technol.* **20** 024003

[10] Joshi R P and Thagard S M 2013 Streamer-Like Electrical Discharges in Water: Part I. Fundamental Mechanisms *Plasma Chem. Plasma Process.* **33** 1–15

[11] Lesaint O 2016 Prebreakdown phenomena in liquids: propagation 'modes' and basic physical properties *J. Phys. D. Appl. Phys.* **49** 144001

[12] Hamdan A, Gorry J, Merciris T and Margot J 2020 Electrical characterization of positive and negative pulsed nanosecond discharges in water coupled with time-resolved light detection *J. Appl. Phys.* **128** 33304

[13] Ushakov V Y 2007 Discharge Propagation in Gaps with a Non-Uniform Field BT - Impulse Breakdown of Liquids ed V Y Ushakov (Berlin, Heidelberg: Springer Berlin Heidelberg) pp 133–237

[14] Bruggeman P and Leys C 2009 Non-thermal plasmas in and in contact with liquids *J. Phys. D. Appl. Phys.* **42** 053001

[15] Qian J, Joshi R P, Schamiloglu E, Gaudet J, Woodworth J R and Lehr J 2006 Analysis of polarity effects in the electrical breakdown of liquids *J. Phys. D. Appl. Phys.* **39** 359–69

[16] Sunka P, Babický V, Clupek M, Lukes P, Simek M, Schmidt J and Cernák M 1999 Generation of chemically active species by electrical discharges in water *Plasma Sources Sci. Technol.* **8** 258–65

[17] Luo Y, Lietz A M, Yatom S, Kushner M J and Bruggeman P J 2018 Plasma kinetics in a nanosecond pulsed filamentary discharge sustained in Ar–H2O and H2O *J. Phys. D. Appl. Phys.* **52** 44003

[18] Malik M A, Ghaffar A and Malik S A 2001 Water purification by electrical discharges *Plasma Sources Sci. Technol.* **10** 82–91

[19] Hamdan A, Agati M and Boninelli S 2020 Selective Synthesis of 2D Mesoporous CuO Agglomerates by Pulsed Spark Discharge in Water *Plasma Chem. Plasma Process.*

[20] Glad X, Profili J, Cha M S and Hamdan A 2020 Synthesis of copper and copper oxide nanomaterials by electrical discharges in water with various electrical conductivities *J. Appl. Phys.* **127** 23302

[21] Hamdan A, Profili J and Cha M S 2020 Microwave Plasma Jet in Water: Effect of Water Electrical Conductivity on Plasma Characteristics *Plasma Chem. Plasma Process.* **49** 169–85

[22] Tachibana K and Nakamura T 2019 Comparative study of discharge schemes for production rates and ratios of reactive oxygen and nitrogen species in plasma activated water *J. Phys. D. Appl. Phys.* **52** 385202

[23] Locke B R and Shih K Y 2011 Review of the methods to form hydrogen peroxide in electrical discharge plasma with liquid water *Plasma Sources Sci. Technol.* **20** 034006

[24] Lukes P, Locke B R and Brisset J-L 2012 Aqueous-Phase Chemistry of Electrical Discharge Plasma in Water and in Gas–Liquid Environments *Plasma Chem. Catal. Gases Liq.* 243–308

[25] Diamond J, Hamdan A, Profili J and Margot J 2020 Time and space-resolved imaging of an AC air discharge in-contact with water *J. Phys. D. Appl. Phys.*

[26] Hamdan A, Ridani D A, Diamond J and Daghrir R 2020 Pulsed nanosecond air discharge in contact with water: influence of voltage polarity, amplitude, pulse width, and gap distance *J. Phys. D. Appl. Phys.* **53** 355202

[27] Diamond J, Profili J and Hamdan A 2019 Characterization of Various Air Plasma Discharge Modes in Contact with Water and Their Effect on the Degradation of Reactive Dyes *Plasma Chem. Plasma Process.* **39** 1483–98

[28] Hamdan A, Čerņevičs K and Cha M S 2017 The effect of electrical conductivity on nanosecond discharges in distilled water and in methanol with argon bubbles *J. Phys. D. Appl. Phys.*

[29] Hamdan A and Cha M S 2016 The effects of gaseous bubble composition and gap distance on the characteristics of nanosecond discharges in distilled water *J. Phys. D. Appl. Phys.* **49** 245203

[30] Hamdan A and Cha M S 2016 Nanosecond Discharge in Bubbled Liquid n-Heptane: Effects of Gas Composition and Water Addition *IEEE Trans. Plasma Sci.* **44** 2988–94

[31] Hamdan A and Cha M S 2015 Ignition modes of nanosecond discharge with bubbles in distilled water *J. Phys. D. Appl. Phys.* **48** 405206

[32] Hamdan A, Liu J L and Cha M S 2018 Microwave Plasma Jet in Water: Characterization and Feasibility to Wastewater Treatment *Plasma Chem. Plasma Process.* **38** 1003–20

[33] García M C, Mora M, Esquivel D, Foster J E, Rodero A, Jiménez-Sanchidrián C and Romero-Salguero F J 2017 Microwave atmospheric pressure plasma jets for wastewater treatment: Degradation of methylene blue as a model dye *Chemosphere* **180** 239–46

[34] Ishijima T, Hotta H, Sugai H and Sato M 2007 Multibubble plasma production and solvent decomposition in water by slot-excited microwave discharge *Appl. Phys. Lett.* **91** 121501

[35] Babaeva N Y and Kushner M J 2009 Structure of positive streamers inside gaseous bubbles immersed in liquids *J. Phys. D. Appl. Phys.* **42** 132003

[36] Babaeva N Y, Tereshonok D V and Naidis G V 2015 Initiation of breakdown in bubbles immersed in liquids: pre-existed charges versus bubble size *J. Phys. D. Appl. Phys.* **48** 355201

[37] Babaeva N Y, Tereshonok D V, Naidis G V and Smirnov B M 2015 Initiation of breakdown in strings of bubbles immersed in transformer oil and water: string orientation and proximity of bubbles *J. Phys. D. Appl. Phys.* **49** 25202

[38] Tu Y, Xia H, Yang Y and Lu X 2016 Time-resolved imaging of electrical discharge development in underwater bubbles *Phys. Plasmas* **23** 13507

[39] Hamdan A and Cha M S 2016 Low-dielectric layer increases nanosecond electric discharges in distilled water *AIP Adv.* **6** 105112

[40] Hamdan A and Cha M S 2018 Carbon-based nanomaterial synthesis using nanosecond electrical discharges in immiscible layered liquids: n-heptane and water *J. Phys. D. Appl. Phys.* **51** 244003

[41] Hamdan A, Abdul Halim R, Anjum D and Cha M S 2017 Synthesis of SiOC:H nanoparticles by electrical discharge in hexamethyldisilazane and water *Plasma Process. Polym.* **14** 1700089

[42] Drake F H, Pierce G W and Dow M T 1930 Measurement of the Dielectric Constant and Index of Refraction of Water and Aqueous Solutions of KCl at High Frequencies *Phys. Rev.* **35** 613–22

[43] Chen T, Hefter G and Buchner R 2003 Dielectric Spectroscopy of Aqueous Solutions of KCl and CsCl *J. Phys. Chem. A* **107** 4025–31

[44] Francis M J 2008 Effect of Degassing on the Electrical Conductivity of Pure Water and Potassium Chloride Solutions *J. Phys. Chem. C* **112** 14563–9

[45] Marinov I L, Guaitella O, Rousseau A and Starikovskaia S M 2011 Successive Nanosecond Discharges in Water *IEEE Trans. Plasma Sci.* **39** 2672–3

[46] Marinov I, Starikovskaia S and Rousseau A 2014 Dynamics of plasma evolution in a nanosecond underwater discharge *J. Phys. D. Appl. Phys.* **47** 224017

[47] Marinov I, Guaitella O, Rousseau A and Starikovskaia S M 2013 Modes of underwater discharge propagation in a series of nanosecond successive pulses *J. Phys. D. Appl. Phys.* **46** 464013

[48] Hamdan A, Marinov I, Rousseau A and Belmonte T 2013 Time-resolved imaging of nanosecond-pulsed micro-discharges in heptane *J. Phys. D. Appl. Phys.* **47** 55203

[49] Hamdan A, Noel C, Kosior F, Henrion G and Belmonte T 2013 Impacts created on various materials by micro-discharges in heptane: Influence of the dissipated charge *J. Appl. Phys.* **113** 43301

[50] Hamdan A, Noël C, Ghanbaja J and Belmonte T 2014 Comparison of Aluminium Nanostructures Created by Discharges in Various Dielectric Liquids *Plasma Chem. Plasma Process.* **34** 1101–14

[51] Descoeudres A, Hollenstein C, Demellayer R and Wälder G 2004 Optical emission spectroscopy of electrical discharge machining plasma *J. Phys. D. Appl. Phys.* **37** 875–82

[52] Descoeudres A, Hollenstein C, Wälder G and Perez R 2005 Time-resolved imaging and spatially-resolved spectroscopy of electrical discharge machining plasma *J. Phys. D. Appl. Phys.* **38** 4066–73

[53] Gigosos M A, González M Á and Cardeñoso V 2003 Computer simulated Balmer-alpha, -

beta and -gamma Stark line profiles for non-equilibrium plasmas diagnostics *Spectrochim. Acta - Part B At. Spectrosc.* **58** 1489–504

[54] Wen X Q, Niu Z W, Hou B and Ren C-S 2015 Experimental measurement of spatially resolved electron density in a filament of a pulsed positive streamer discharge in water *Appl. Phys. Lett.* **106** 264101

[55] Niu Z, Wen X, Ren C and Qiu Y 2016 Measurement of Temporally and Spatially Resolved Electron Density in the Filament of a Pulsed Spark Discharge in Water *Plasma Sci. Technol.* **18** 821–5

[56] Merciris T, Valensi F and Hamdan A 2020 Determination of the Electrical Circuit Equivalent to a Pulsed Discharge in Water: Assessment of the Temporal Evolution of Electron Density and Temperature *IEEE Trans. Plasma Sci.* **48** 3193–202

[57] Šunka P 2001 Pulse electrical discharges in water and their applications *Phys. Plasmas* **8** 2587–94

[58] Liu S-W, Liu Y, Ren Y-J, Lin F-C, Li H and Zhao Y 2020 Influence of conductivities on electrical breakdown of water under microsecond pulsed voltage *Phys. Plasmas* **27** 63512

[59] Naidis G V 2015 Modeling of subnanosecond discharge in hydrocarbon liquid *IEEE Transactions on Plasma Science **43*** 3138-3141.